

1 **Estimating the sensitivity of the Priestley-Taylor coefficient to air**
2 **temperature and humidity**

3 Ziwei Liu, Hanbo Yang *, Changming Li, Taihua Wang

4 State Key Laboratory of Hydro-science and Engineering, Department of Hydraulic
5 Engineering, Tsinghua University, Beijing, China

6 *Correspondence to:* Hanbo Yang (yanghanbo@tsinghua.edu.cn)

7 Abstract

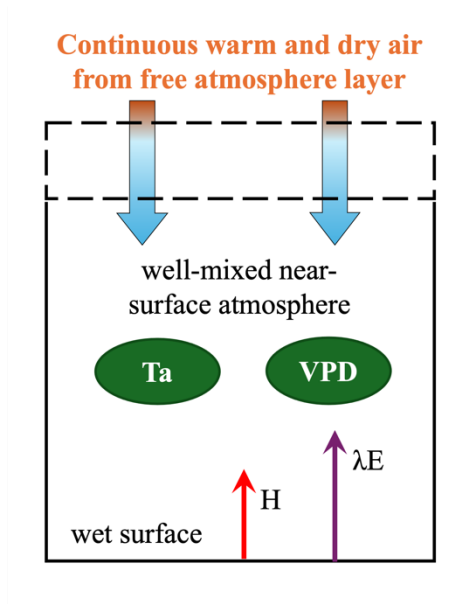
8 Priestley-Taylor (PT) coefficient (α) is generally set as a constant value or fitted as an
9 empirical function of environmental variables, and it can bias the evaporation estimation
10 or hydrological projections under global warming. By using an atmospheric boundary
11 layer model, this study derives a theoretical and parameter-free equation for estimating α
12 as a function of air temperature (T) and specific humidity (Q). With observations from
13 several water bodies and non-water-limited land sites, we demonstrate that in addition to
14 well estimating the value of α , the derived expressions can also capture the sensitivity of
15 α to T and Q, that is, $d\alpha/dT$ and $d\alpha/dQ$. α is generally negatively associated with T and Q,
16 of which T plays a more fundamental role in controlling α behaviors. Based on climate
17 model data, we further show that this negative relationship between α and T is of great
18 importance for long-term hydrological predictions. We also provide a lookup graph for
19 practical and broad uses to directly find the values of $d\alpha/dT$ and $d\alpha/dQ$ under specific
20 conditions. Overall, the derived expression gives a physically clear and straightforward
21 approach to quantify changes in α , which is essential for PT-based hydrological
22 simulation and projections.

23 **1. Introduction**

24 Evaporation from wet surfaces, including oceans, lakes, and reservoirs, is relevant to
 25 global hydrological cycles and water availability. There is a long history of developing
 26 theories and methods to estimate wet surface evaporation (Bowen, 1926; Penman, 1948;
 27 Priestley and Taylor, 1972; Thornthwaite and Holzman, 1939; Yang and Roderick, 2019).
 28 Among existing models, the Priestley-Taylor (PT) model/equation is known for its
 29 transparent structure and low input requirement (Priestley and Taylor, 1972). The PT
 30 equation is widely used in evaporation estimation across varied scales and is the basis for
 31 various hydrologic and land surface models. Specifically, the PT equation comes from
 32 the equilibrium evaporation (λE_{eq}), and λE_{eq} can be calculated as (Slatyer and Mcilroy,
 33 1961):

34
$$\lambda E_{eq} = \frac{\epsilon_a}{\epsilon_a + 1} (R_n - G) \quad (1)$$

35 where λ (J/kg) is the latent heat of water vaporization, $\epsilon_a = \Delta/\gamma$, Δ (kPa/K) is the slope of
 36 the saturated vapor pressure versus temperature curve (a function of temperature), and γ
 37 is the psychrometric constant. ϵ_a is a function of air temperature (T). $R_n - G$ (kPa/K) is the
 38 available energy. The equilibrium evaporation indicates that the near-surface air is
 39 saturated, supposing the vapor pressure deficit (VPD) is zero. However, it does not exist
 40 in the real world (Brutsaert and Stricker, 1979; Lhomme, 1997a), due to the continuous
 41 exchanges of warm and dry air from the entrainment layer, although water is continuously
 42 transported from the bottom wet surface into the atmosphere through the evaporation
 43 process (Figure 1).



44
 45 Figure 1. Atmospheric boundary layer box model describing the energy and water fluxes
 46 at the saturated surface and atmosphere above. The dotted line represents the removable
 47 upper boundary of the box. H and λE are the sensible and latent heat fluxes. T_a is the air

48 temperature and VPD is the vapor pressure deficit.

49

50 In this case, the PT equation introduced a parameter, α , known as the PT coefficient, to
51 estimate wet surface evaporation (Priestley and Taylor, 1972). α represents the effects of
52 vertical mixing of dry and moist air and adjusts the equilibrium evaporation to the actual
53 evaporation. So qualitatively speaking, the α is impossibly lower than one because the air
54 is always not saturated and can only infinitely close to saturated condition, no matter how
55 moist the near-surface air is. The PT equation is:

$$56 \quad \lambda E = \alpha \frac{\varepsilon_a}{\varepsilon_a + 1} (R_n - G) \quad (2)$$

57 In the original study of Priestley and Taylor (1972), the value of α is fitted as 1.26. While
58 a fixed α value can reasonably estimate wet surface evaporation (Yang and Roderick,
59 2019), some studies found that α varies across time and space, for example, α often shows
60 a more prominent value under cold conditions and becomes lower as warms (Xiao et al.,
61 2020; Debruin and Keijman, 1979). This indicates that α should be a variable rather than
62 a constant (Assouline et al., 2016; Guo et al., 2015; Jury and Tanner, 1975; Lhomme,
63 1997b; Van Heerwaarden et al., 2009; Eichinger et al., 1996; Mcnaughton and Spriggs,
64 1986; Crago et al., 2023; Maes et al., 2019). However, the hydrology field predominantly
65 employs the fixed value of $\alpha = 1.26$, despite those earlier findings being over three
66 decades old.

67 A general method to quantify the changes in α is to inverse it with observations based on
68 Equation (2) and then build relationships among α and investigated variables. Since a
69 negative relationship between α and temperature (T) is a consensus from multi-scale
70 observations (Assouline et al., 2016; Xiao et al., 2020), many attempts empirically fitted
71 α as a function of T (Andreas and Cash, 1996; Hicks and Hess, 1977; Yang and Roderick,
72 2019). Recent work further showed that the air humidity state can also influence the
73 spatiotemporal patterns of α (Su and Singh, 2023). While those methods promote our
74 understanding of the potential variations in α , they more lie on the empirical side and pay
75 less attention to the underlying process. Hence, various endeavors have been made to
76 calculate α through physical means, but they are often constrained by the complexity of
77 numerous parameters. For instance, in the research conducted by Lhomme (1997b), α was
78 explicitly formulated utilizing the PM model in conjunction with boundary layer theory.
79 Nevertheless, the formulation incorporates parameters that signify surface and
80 aerodynamic resistances, making them hard to determine through direct measurements.
81 Subsequently, by using a refined boundary layer model, Van Heerwaarden et al. (2009)
82 introduced a mathematical expression for estimating α , however, the expression also
83 involves a set of parameters necessitating numerical experiments to delineate a feasible
84 range for α . Consequently, obtaining a precise α estimation using conventional
85 observations still has remained a challenge.

86 Based on a recent study by Liu and Yang (2021), here we aim to derive a physically clear,
 87 transparent, and calibration-free equation for estimating α , by introducing a governing
 88 equation (potential vapor pressure deficit budget) into the conventional boundary layer
 89 model. In the following sections, we will first provide the theory for estimating α and its
 90 sensitivity to climate conditions: air temperature (T) and humidity (represented by the air
 91 specific humidity, Q). We further evaluate the theory based on measurements from the
 92 water and non-water-limited land surfaces, followed by the influences of α changes on
 93 long-term hydrologic projections.

94 2. Theory

95 2.1 Derivation of Bowen ratio

96 Here, we use an atmospheric boundary layer-based (ABL) model as the basis for the
 97 Bowen ratio (defined as the ratio of sensible heat fluxes to latent heat fluxes, $H/\lambda E$)
 98 derivation (Liu and Yang, 2021). The fundamental conservation equations for states of
 99 moisture and energy over the water surfaces are (Raupach, 2001):

$$100 \quad \rho c_p \frac{d\theta}{dt} = \frac{H}{h} + \frac{\rho c_p g_e}{h} (\theta_e - \theta) \quad (3)$$

$$101 \quad \rho \lambda \frac{dQ}{dt} = \frac{\lambda E}{h} + \frac{\rho \lambda g_e}{h} (Q_e - Q) \quad (4)$$

102 where θ (K) is the potential temperature, Q is the specific humidity, c_p (J/kg/K) is the
 103 specific heat capacity of air at constant pressure, g_e (m/s) is the entrainment flux velocity
 104 into the ABL box, and h (m) is the height of the ABL. The subscript e indicates the
 105 variable is evaluated at the upper boundary of the ABL (see Figure 1).

106 According to Equations (3) and (4), we can obtain a formula to calculate the rate of VPD
 107 ($dVPD/dt$, see details in Liu and Yang (2021)):

$$108 \quad \frac{dVPD}{dt} = \frac{\epsilon_a H - \lambda E}{\rho \lambda h} + \frac{g_e}{h} \Delta_D \quad (5)$$

109 where Δ_D is calculated as:

$$110 \quad \Delta_D = VPD_e - VPD \quad (6)$$

111 Under the state that air is saturated, the water vapor is continuously transported from the
 112 water surface to the atmosphere, keeping the air saturated. In this case, there is no vertical
 113 moisture gradient, that is, the air near the surface and the air at the upper boundary of the
 114 ABL should be saturated, so VPD and VPD_e are both equal to zero. With Equation (6),
 115 we can know $\Delta_D = 0$.

116 When air is not saturated, we can rewrite Equation (6) as:

$$117 \quad \Delta_D = Q - Q_e + [Q_{\text{sat}}(\theta_e) - Q_{\text{sat}}(\theta)] \quad (7)$$

118 where Q_e is much smaller than Q , and $Q_{\text{sat}}(\theta_e) - Q_{\text{sat}}(\theta)$ is small (one order of magnitude
119 smaller than Q), so the Δ_D roughly equals Q (Raupach, 2001; Liu and Yang, 2021).

120 Under a relatively long-term (monthly and/or longer), there is a potential VPD budget
121 ($d\text{VPD}/dt = 0$) over water surfaces (Raupach, 2001), and g_e can be estimated as the
122 function of H and λE as:

$$123 \quad g_e = \frac{H + \Lambda \cdot \lambda E}{\rho c_p \gamma_v h} \quad (8)$$

124 where Λ is a constant (0.07), and γ_v is the potential virtual temperature gradient in the
125 free atmosphere above the ABL. $\gamma_v h$ can be set as a fixed value of 7 K (Liu and Yang,
126 2021). Combining with the VPD budget, Equation (5) and (8), we can obtain the
127 expression for Bo :

$$128 \quad Bo = \begin{cases} \frac{1}{\varepsilon_a}, \text{equilibrium} \\ \frac{1 - \Lambda \chi}{\varepsilon_a + \chi}, \text{non-equilibrium} \end{cases} \quad (9)$$

129 where $\chi = \frac{\lambda Q}{c_p \gamma_v h}$, a function of Q .

130 **2.2 Theoretical formula for α**

131 The surface energy balance is expressed as:

$$132 \quad R_n = H + \lambda E + G = (1 + Bo)\lambda E + G. \quad (10)$$

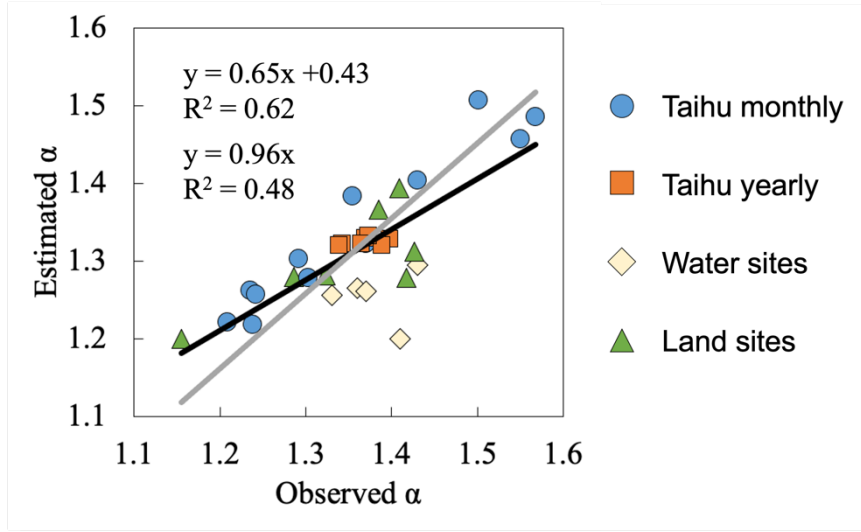
133 Combining Equations (2) and (10), α can be calculated as:

$$134 \quad \alpha = \frac{1}{1 + Bo} \frac{\varepsilon_a + 1}{\varepsilon_a}. \quad (11)$$

135 With Equation (9) and (11), we can derive the formula for α :

$$136 \quad \alpha = \begin{cases} 1, \text{equilibrium} \\ 1 + \frac{(\varepsilon_a \Lambda + 1)\chi}{\varepsilon_a [\varepsilon_a + 1 + (1 - \Lambda)\chi]}, \text{non-equilibrium} \end{cases} \quad (12)$$

137 Equation (12) is one of the main results in this study, and it can estimate α well compared
 138 to a large number of observations (Figure 2, please see the description of observed data
 139 in Section 3).



140
 141 Figure 2. Comparison between observed and Equation (12) calculated α . The black line
 142 is the linear fitting with intercept and the gray line is the linear fitting through origin. The
 143 observed α is inversed by the PT model.

144 2.3 The sensitivity of α to air temperature and humidity

145 According to the above derivations, we can know that α is not a constant and it changes
 146 with T and Q. The sensitivity of α to T and Q, $d\alpha/dT$ and $d\alpha/dQ$, determines the variation
 147 of α if the initial α value is given. In this section, we derive explicit equations to estimate
 148 $d\alpha/dT$ and $d\alpha/dQ$.

149 Firstly, we decompose α changes in that of T and Q with partial differential equations
 150 based on Equation (11):

$$151 \quad \frac{\partial \alpha}{\partial T} = -\frac{1}{(1 + \text{Bo}_{\text{ABL}})^2} \frac{\varepsilon_a + 1}{\varepsilon_a} \frac{\partial \text{Bo}_{\text{ABL}}}{\partial T} - \frac{1}{\varepsilon_a^2} \frac{1}{1 + \text{Bo}_{\text{ABL}}} \frac{\partial \varepsilon_a}{\partial T}, \quad (13)$$

$$152 \quad \frac{\partial \alpha}{\partial Q} = -\frac{1}{(1 + \text{Bo}_{\text{ABL}})^2} \frac{\varepsilon_a + 1}{\varepsilon_a} \frac{\partial \text{Bo}_{\text{ABL}}}{\partial Q}, \quad (14)$$

153 where partial differential terms of $\frac{\partial \text{Bo}_{\text{ABL}}}{\partial T}$ and $\frac{\partial \text{Bo}_{\text{ABL}}}{\partial Q}$ can be estimated based on

154 Equation (9) as:

$$155 \quad \frac{\partial \text{Bo}_{\text{ABL}}}{\partial T} = -\frac{1 - \Lambda \chi}{(\varepsilon_a + \chi)^2} \frac{\partial \varepsilon_a}{\partial T}, \quad (15)$$

$$156 \quad \frac{\partial \text{Bo}_{\text{ABL}}}{\partial Q} = -\frac{\Lambda \varepsilon_a + 1}{(\varepsilon_a + \chi)^2} \frac{\partial \chi}{\partial Q}. \quad (16)$$

157 where terms of $\frac{\partial \varepsilon_a}{\partial T}$ and $\frac{\partial \chi}{\partial Q}$ can be approximated as:

$$158 \quad \frac{\partial \varepsilon_a}{\partial T} = \frac{1}{\gamma} \frac{\partial \Delta}{\partial T}, \quad (17)$$

$$159 \quad \frac{\partial \chi}{\partial Q} = \frac{\lambda}{c_p \gamma_v h}, \quad (18)$$

160 where Δ can be calculated as:

$$161 \quad \Delta = \frac{4098 e_s}{(T + 237.3)^2}. \quad (19)$$

162 Combining Equation (13)-(18), we can obtain:

$$163 \quad \frac{\partial \alpha}{\partial T} = \frac{1}{\gamma} \left[\frac{1}{(1 + \text{Bo}_{\text{ABL}})^2} \frac{1 - \Lambda \chi}{(\varepsilon_a + \chi)^2} \frac{\varepsilon_a + 1}{\varepsilon_a} - \frac{1}{\varepsilon_a^2} \frac{1}{1 + \text{Bo}_{\text{ABL}}} \right] \frac{\partial \Delta}{\partial T} \quad (20)$$

$$164 \quad \frac{\partial \alpha}{\partial Q} = \frac{1}{(1 + \text{Bo}_{\text{ABL}})^2} \frac{\Lambda \varepsilon_a + 1}{(\varepsilon_a + \chi)^2} \frac{\varepsilon_a + 1}{\varepsilon_a} \frac{\lambda}{c_p \gamma_v h} \quad (21)$$

165 We can rewrite the Equation (20) as follows:

$$166 \quad \frac{\partial \alpha}{\partial T} = -\frac{1}{\gamma} \frac{\chi \left[\varepsilon_a (\Lambda \varepsilon_a + 2) + \chi (1 - \Lambda) + 1 \right]}{(1 + \text{Bo}_{\text{ABL}})^2 (\varepsilon_a + \chi)^2 \varepsilon_a^2} \frac{\partial \Delta}{\partial T}, \quad (22)$$

167 The total differentiation of α is:

$$168 \quad d\alpha = \frac{\partial \alpha}{\partial T} dT + \frac{\partial \alpha}{\partial Q} dQ, \quad (23)$$

169 thus $\frac{d\alpha}{dT}$ and $\frac{d\alpha}{dQ}$ can be written as:

$$170 \quad \frac{d\alpha}{dT} = \frac{\partial \alpha}{\partial T} + \frac{\partial \alpha}{\partial Q} \frac{dQ}{dT}, \quad (24)$$

$$171 \quad \frac{d\alpha}{dQ} = \frac{\partial \alpha}{\partial Q} + \frac{\partial \alpha}{\partial T} \frac{dT}{dQ}. \quad (25)$$

172 With the above equations, we can get theoretical relationships among α , T , and Q . This
 173 derivation can provide a simple and physically clear estimation for α changes. We also
 174 obtained da/dT and da/dQ values by fitting measured data using the linear regression

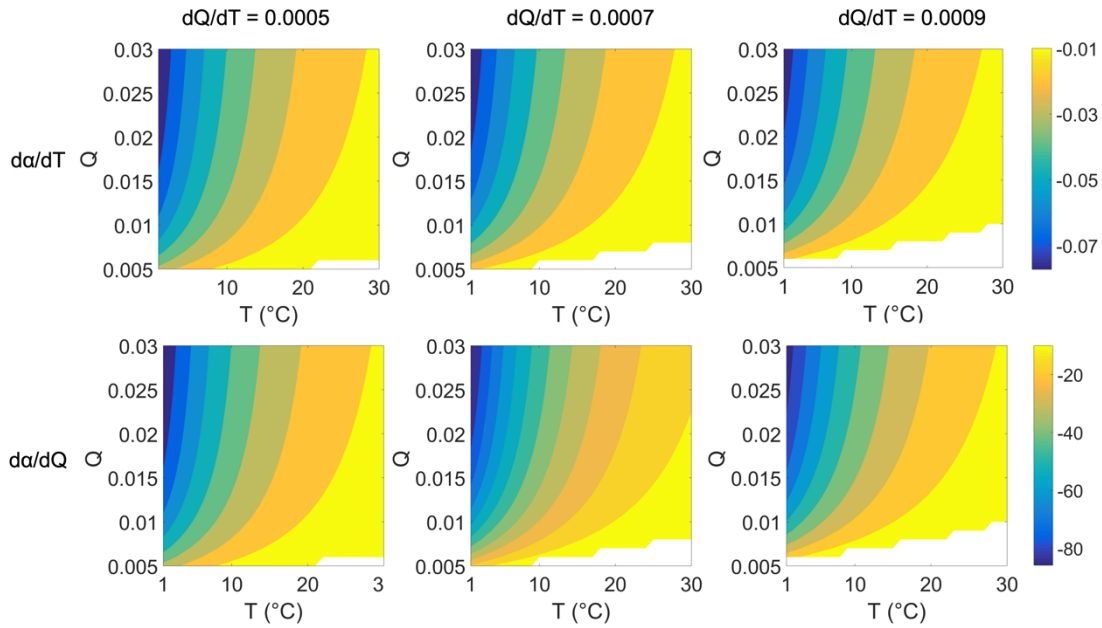
175 model.

176 For practical use, we simplified the Equation (20) and (21) as:

$$177 \quad \frac{\partial \alpha}{\partial T} = -\frac{1}{\gamma} \frac{\chi}{\varepsilon_a} \frac{1}{\varepsilon_a + \chi} \frac{\partial \Delta}{\partial T} \quad (26)$$

$$178 \quad \frac{\partial \alpha}{\partial Q} = \frac{\varepsilon_a + 1}{\varepsilon_a (\varepsilon_a + \chi + 1)^2} \frac{\chi}{Q} \quad (27)$$

179 We further gave a numerical plot to show how α changes with T and Q (Figure 3). We
 180 plot this figure by setting a dQ/dT gradient from 0.0005, 0.0007, and 0.0009/K to ensure
 181 cover most of the cases over water surfaces. Figure 3 can be used as the lookup graphs to
 182 directly find da/dT and da/dQ values. For example, for a water surface with dQ/dT
 183 about 0.0007 /K, the values of da/dT and da/dQ can be found in the second column
 184 of Figure 3.



185

186 Figure 3. Values of da/dT and da/dQ under different T and Q . The first and second
 187 rows are da/dT and da/dQ , respectively. The first to third columns are under different
 188 correlations between Q and T (dQ/dT) as 0.0005, 0.0007, and 0.0009/K, respectively.
 189 The blank space in each subpanel refers to values of da/dT and da/dQ are negative,
 190 indicating situations that rarely happen in the real world (i.e., with a very high temperature,
 191 the specific humidity is hardly deficient over wet surfaces).

192 3. Cases and applications

193 3.1 Data

194 We select data from eddy covariance measurements on several water surfaces (Han and
 195 Guo, 2023): (i) Lake Taihu, located in the Yangtze River Delta, China, with an area of
 196 $\sim 2,400 \text{ km}^2$, an average depth of 1.9 m (Lee et al., 2014). There are five sites over the
 197 Taihu surface, and the poor-quality data marked with quality flags are removed. (ii) Lake
 198 Poyang, located in the Yangtze Plain, China, with an area of $\sim 3,000 \text{ km}^2$ and an average
 199 depth of 8.4 m (Zhao and Liu, 2018). (iii) Erhai, located in the Yun-Gui Plateau of China,
 200 with an area of $\sim 250 \text{ km}^2$ and an average depth of 10 m (Du et al., 2018). (iv) Guandu
 201 Ponds, located in Anhui Province, China, with an area of $\sim 0.05 \text{ km}^2$ and an average depth
 202 of 0.8 m (Zhao et al., 2019); (v) Lake Suwa, located in Nagano, Japan, with an area of
 203 $\sim 13 \text{ km}^2$ and an average depth of 4 m (Taoka et al., 2020). Months with negative values
 204 of sensible heat fluxes have not remained. Given the absence of observed heat storage (G)
 205 at some sites, we use the sum of latent heat flux and sensible heat flux (i.e., $LE+H$) instead
 206 of net radiation minus G (R_n-G) as the measure of available energy. Using either $LE+H$
 207 or R_n-G yields identical results, as our objective is to use the available energy to invert
 208 parameter α from observations. The latitude, longitude, and available data period of five
 209 lakes/ponds are listed in Table 1. For α changes in time, we use data from Lake Taihu for
 210 investigation due to its sufficient data length. For α changes in space, we calculate the
 211 average temperature, specific humidity, and α of each lake for comparison.

212 Table 1. Location and date period of each water body.

Site	Lat ($^{\circ}$)	Lon ($^{\circ}$)	Size (km^2)	Periods ^a	Sample size (number of months)
Taihu	31.23	120.11	3000	2012.01 - 2018.12	341 ^b
Poyang	29.08	116.40	2400	2013.08 - 2017.09	41
Erhai	25.77	100.17	250	2012.01 - 2018.12	24 ^c
Guandu	31.97	118.25	0.05	2017.06 - 2019.12	31
Suwa	36.05	138.11	13	2016.01 - 2018.12	36

213 Note: a. Periods refer to the date of the first measurement to the date of the last one,
 214 including months for which no data are available. b. There are five eddy covariance
 215 sites over lake Taihu. c. Only climatology monthly data from two periods of 2012-2015
 216 and 2015-2018 are available.

217 Observations from global flux sites (FluxNet2015 database) are also selected. We first
 218 examine days without water stress based on the following steps (Maes et al., 2019). At
 219 each site, the evaporative fraction (i.e., EF, latent heat flux over the sum of latent and
 220 sensible fluxes) is first calculated, and the days with EF exceeding the 95th percentile EF
 221 and with EF larger than 0.8 remain. Secondly, the days with soil moisture lower than 50%

222 of the maximum soil moisture (taken as the 98th percentile of the soil moisture series) are
 223 removed. Days having rainfall and negative values of latent and sensible heat fluxes are
 224 also not included. As a result, a total of ~ 700 non-water-stressed site-days pass the
 225 criterion. Data is divided into seven vegetation types including croplands (CRO),
 226 wetlands (WET), evergreen needleleaf and mixed forests (DNF_MF), evergreen
 227 broadleaf and deciduous broadleaf forests (EBF_DBF), grasslands (GRA), close
 228 shrublands (CSH), and woody savanna (WSA), to analyze α changes in space. It should
 229 be noted that we do not average the daily data to a monthly scale due to variations in data
 230 sizes across different months for a specific site. Instead, we organize the selected daily
 231 data by vegetation types, as the primary objective of utilizing land fluxes data is to assess
 232 the derived relationship spatially rather than temporally.

233 We also collect ocean surface data from 11 CMIP6 models (under scenario SSP585, Table
 234 2) from 2021-2100 to see the temporal changes in α . The calculation is limited to the
 235 latitudinal range 60°S to 60°N , and takes all ocean surface grids as a whole (Roderick et
 236 al., 2014). We average the monthly data to the yearly scale and calculate α every ten years
 237 from 2021 to 2100 (i.e., 2021-2030, 2031-2040, etc.).

238 Table 2. CMIP6 models used in this study.

Model	Nation	Institute
ACCESS-ESM1-5	Australia	CSIRO
CanESM5	Canada	CCCma
CESM2-WACCM	USA	NCAR
CMCC-CM2-SR5	Italy	CMCC
CMCC-ESM2	Italy	CMCC
FGOALS-g3	China	CAS
FIO-ESM-2-0	China	CAS
MPI-ESM1-2-HR	Germany	MPI-M
MPI-ESM1-2-LR	Germany	MPI-M
NorESM2-LM	Norway	NCC
NorESM2-MM	Norway	NCC

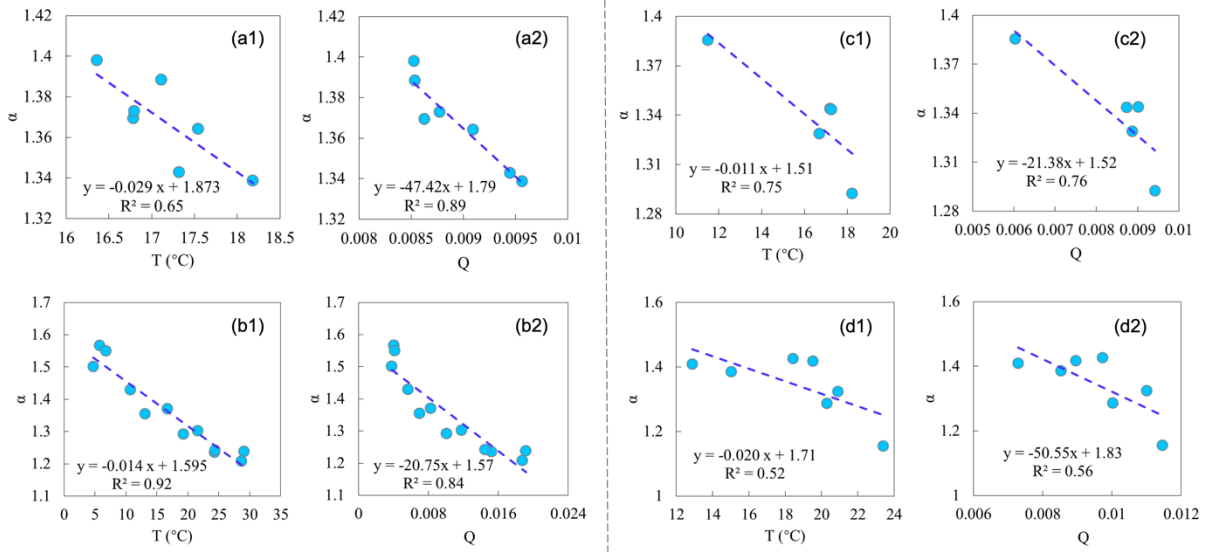
239 Note: CSIRO: Commonwealth Scientific and Industrial Research Organization;
 240 CCCma: Canadian Centre for Climate Modelling and Analysis; NCAR: National Center
 241 for Atmospheric Research; CMCC: Euro-Mediterranean Center on Climate Change;
 242 CAS: Chinese Academy of Sciences; MPI-M: Max Planck Institute for Meteorology;
 243 NCC: Norwegian Climate Centre.

244 3.2 Results

245 (1) Temporal and spatial changes in α

246 We used yearly and climatology monthly (from Jan to Dec) data from Lake Taihu to

247 investigate the temporal variation in α . α is firstly inversed by the PT model and
 248 measurements, and then we found significant negative relationships of α with both T and
 249 Q (Figure 4). On the yearly scale, the regressed values of $d\alpha/dT$ and $d\alpha/dQ$ are -
 250 0.029/ $^{\circ}\text{C}$ and -47.42, and the values on the seasonal scale are -0.014/ $^{\circ}\text{C}$ and -20.75,
 251 respectively. $d\alpha/dT$ on the seasonal scale is higher than that on the yearly scale because
 252 the variation range of α on the seasonal scale is more extensive. Theoretical derivations
 253 can roughly reproduce the sensitivity of α to T and Q, although there is some potential
 254 uncertainty from interannual variations (Table 3). We also analyzed the results on the ten-
 255 day scale and obtained similar findings (see Appendix Figure A1 and Table A1).



256
 257 Figure 4. Temporal and spatial relationships of α and temperature (T) and specific
 258 humidity (Q). (a-b) Temporal relationships based on Lake Taihu data: (a) yearly data, and
 259 (b) climatology monthly data. (c-d) Spatial relationships: (c) data from five water surface
 260 sites, and (d) land surface data from FluxNet2015, each circle representing one vegetation
 261 type. The linear regression line and correlation coefficient (R^2) are shown in each
 262 subpanel.

263
 264 Table 3 Sensitivity of α to temperature (T) and specific humidity (Q) by regression and
 265 theoretical derivation.

		$d\alpha/dT$ ($^{\circ}\text{C}$)		$d\alpha/dQ$	
		regression	derivation	regression	derivation
Temporal	yearly	-0.029	-0.016	-47.42	-20.33
	seasonally	-0.014	-0.011	-20.75	-18.38
Spatial	water sites	-0.011	-0.009	-21.38	-12.22
	land sites	-0.020	-0.013	-50.55	-31.97

266
 267 Spatial relationships of α with T and Q are similar to that in time, i.e., higher T and Q
 268 generally correspond to lower α , supported by measurements over both water and land

269 surfaces (Figure 4). For the water surfaces, the values of $d\alpha/dT$ and $d\alpha/dQ$ are -
 270 0.011/°C and -21.38, and the values for land surfaces are -0.020/°C and -50.55. The
 271 derived $d\alpha/dT$ and $d\alpha/dQ$ matched roughly well with the regressed values, despite
 272 more or less errors (Table 3). The correlations (represented by R^2 in Figure 4) between α
 273 and T, α and Q of water surfaces are higher than those over the land surfaces. This
 274 indicates that changes in α are more associated with T and Q over water surfaces, which
 275 may be because T and Q dominate the water surface evaporation process, while some
 276 other factors, like vegetation and wind speed, also play specific roles over land surfaces.

277 Based on Equation (20) to (22), $\partial\alpha/\partial T$ is always a negative value, and $\partial\alpha/\partial Q$ is
 278 always positive. The regressed and derived $d\alpha/dT$ and $d\alpha/dQ$ are both negative.
 279 Combined with Equations (24), (25) and the positive relationship between T and Q, the
 280 $\partial\alpha/\partial T$ plays a more critical role in determining (the signs of) $d\alpha/dT$ and $d\alpha/dQ$, that
 281 is, $|\partial\alpha/\partial T| > \partial\alpha/\partial Q \cdot dQ/dT$ and $|\partial\alpha/\partial T \cdot dT/dQ| > \partial\alpha/\partial Q$. Specifically, based on the data
 282 from lake Taihu (for detecting α changes in time) and data from different water surface
 283 sites and land surface sites (for detecting α changes in space), we found the contribution
 284 of $\partial\alpha/\partial T \cdot dT$ to $d\alpha$ is ~70%, much more significant than that of $\partial\alpha/\partial Q \cdot dQ$ of ~30%
 285 (Table 4). Therefore, according to the evaporation process over the wet surface (Section
 286 2.1) and the above analyses, we can conclude that α is fundamentally controlled by T and
 287 modulated by Q.

288 Table 4. Contributions of changes in temperature (T) and specific humidity (Q) to
 289 changes in α .

		$d\alpha$	contribution of $\frac{\partial\alpha}{\partial T}dT$	contribution of $\frac{\partial\alpha}{\partial Q}dQ$
Temporal	yearly	-0.029	70%	30%
	seasonally	-0.256	66%	34%
Spatial	water sites	-0.080	70%	30%
	land sites	-0.136	74%	26%
Average		----	70%	30%

290 Note: Since $d\alpha = \frac{\partial\alpha}{\partial T}dT + \frac{\partial\alpha}{\partial Q}dQ$, the contribution of $\frac{\partial\alpha}{\partial T}dT$ is calculated as

291 $\left| \frac{\partial\alpha}{\partial T}dT \right| / \left| \frac{\partial\alpha}{\partial T}dT + \frac{\partial\alpha}{\partial Q}dQ \right|$, and is the contribution of $\frac{\partial\alpha}{\partial Q}dQ$ calculated as

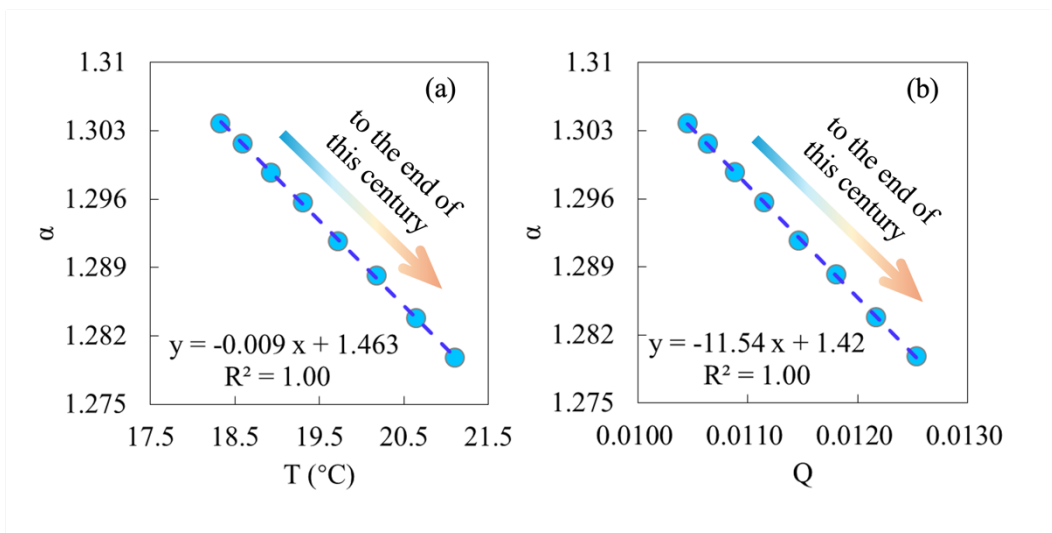
292 $\left| \frac{\partial\alpha}{\partial Q}dQ \right| / \left| \frac{\partial\alpha}{\partial T}dT + \frac{\partial\alpha}{\partial Q}dQ \right|$. $d\alpha$ refers to the estimated variation of α from lowest to highest

293 T (also from lowest to highest Q since T and Q are generally positively correlated).

294 Derived $d\alpha/dT$ and $d\alpha/dQ$ have more or less errors compared to the regressed values.
 295 Several reasons can explain this: (i) errors in measurements of eddy covariance systems;
 296 (ii) the additional factors other than T and Q, like wind speed, can also influence α ; (iii)
 297 the relationship of α and T (also α and Q) cannot be well represented by the linear
 298 regression model. Besides, the water surface size effects on evaporation and α , reported
 299 by Han and Guo (2023), are not well considered in the presented derivation. Nevertheless,
 300 the derived expression can fairly match the observations of water bodies with various
 301 sizes (Table 3).

302 **(2) Potential applications for global projections**

303 Based on CMIP6 ocean surface data, we also detected significant negative relationships
 304 of α with T and Q (Figure 5). $d\alpha/dT$ and $d\alpha/dQ$ obtained by the linear regression are -
 305 0.009/°C and -11.54, respectively. The derived $d\alpha/dT$ and $d\alpha/dQ$ are close to the
 306 regressed value as -0.009/°C and -10.74. We further compared the changes in T, Q, and
 307 heat fluxes between the first and the last ten years in 2021-2100 (Table 5). To the end of
 308 this century, CMIP6 models predict that ocean average available energy (R_n-G) and latent
 309 heat flux (also evaporation) will increase by $\sim 3.1 \text{ W/m}^2$ and $\sim 6.0 \text{ W/m}^2$, respectively.
 310 Using the PT model with the fixed α (1.26), predicted evaporation shows an increase of
 311 $\sim 8.0 \text{ W/m}^2$, far higher than climate models' direct output (with a relative bias of $\sim 30\%$).
 312 Based on derived α , ocean evaporation shows a much smaller increase of $\sim 5.8 \text{ W/m}^2$, with
 313 less than 5% relative bias compared to CMIP6 values (Figure 6). This indicates that
 314 changes in α should be well considered for the long-term projections. So here we suggest
 315 introducing the negative relationship between α and T, proposed in this study, into the
 316 original PT model to correct for the overestimated sensitivity of evaporation to
 317 temperature (Liu et al., 2022), which could also improve the reliability of global long-
 318 term drought predictions (Greve et al., 2019).



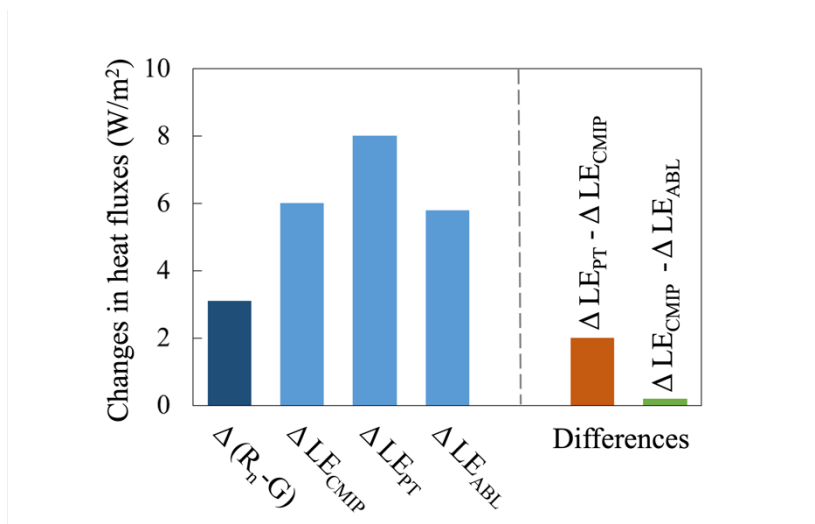
319
 320 Figure 5. Temporal relationship of (a) α and temperature (T), and (b) α and specific

321 humidity (Q) over global ocean surfaces. Each dot denotes the data in each 10-year
 322 window (2021-2030, 2031-2041, ..., 2091-2100), from left to right is from 2021-2030 to
 323 2091-2100.

324
 325 Table 5. Ocean surface temperature, specific humidity, and heat fluxes at the first ten
 326 years (2021-2030) and the end of the 21st century (2091-2100). T, Q, R_n-G, and LE are
 327 direct outputs of climate models. α -CMIP refers to α inverted by the PT model with CMIP
 328 data. LE_{PT} is calculated by the PT model with fixed α at 1.26. α -ABL refers to α estimated
 329 by the ABL model. LE_{ABL} is calculated by the PT model with α -ABL.

Period	T (°C)	Q (-)	R _n -G (W/m ²)	LE (W/m ²)	α -CMIP	LE _{PT} (W/m ²)	α -ABL	LE _{ABL} (W/m ²)
2021-2030	18.1	0.010	122.9	106.8	1.304	103.2	1.316	107.7
2091-2100	21.1	0.013	126.0	112.9	1.279	111.2	1.287	113.5
Δ	3.0	0.003	3.1	6.1	-0.025	8.0	-0.029	5.8

330



331

332 Figure 6. Stylized diagram showing the average changes in heat fluxes over global
 333 ocean surfaces.

334 4. Discussions and Conclusions

335 In this study, we employed an open boundary layer model with a governing potential VPD
 336 budget (Raupach, 2001, 2000), originally integrated by Liu and Yang (2021), to formulate
 337 an expression for the Priestley-Taylor coefficient, α . Notably, the governing equation
 338 allows the derived expression to have no calibrated parameters and can estimate a precise
 339 α value with normal observations, rendering it superior to other methods that are also built
 340 with the boundary layer theory (Lhomme, 1997b; Van Heerwaarden et al., 2009). With
 341 the expression and a variety of measurements, we further demonstrated that temperature
 342 exerts a more significant influence on variations in α , as opposed to specific humidity. We
 343 suggest that for studies focusing on evaporation and/or drought projections, it is crucial

344 to thoroughly characterize the negative correlation between α and temperature, a
 345 relationship easily determined using the derived expression.

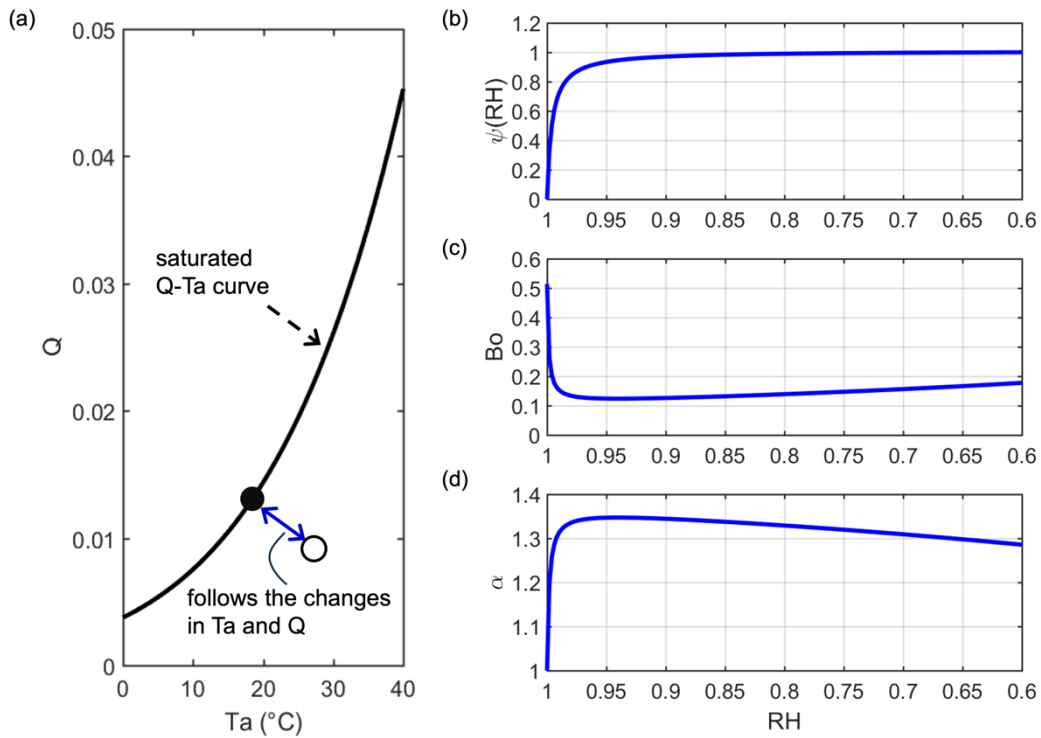
346 It should be noted that except for the PT model, the PM-based model can be also used to
 347 estimate wet surface evaporation (Penman, 1948; Shuttleworth, 1993). While PM-based
 348 equations encapsulate all processes that possibly affect evaporation, the PT model, taking
 349 evaporation as a simple function of radiation and temperature, takes more account of the
 350 feedback/balance between the surface and near atmosphere (Figure 1). Besides, it has
 351 been noted that the PM-based models may fail at certain limits, and cannot capture the
 352 sensitivity of evaporation to temperature changes (Liu et al., 2022; McColl, 2020). So in
 353 this case, also with the fact that the PT model is currently one of the most popular
 354 equations due to its low input requirements, revisiting this classic model can greatly
 355 promote its adaption under the changing climate. Meanwhile, some revised PT equations
 356 can also be used to estimate the parameter α (Yang and Roderick, 2019; De Bruin and
 357 Holtslag, 1982). However, these modifications often exhibit significant deviations
 358 (Figure A2). Specifically, the model developed by De Bruin and Holtslag (1982) is based
 359 on data from one specific site in the Netherlands, and the model built by Yang and
 360 Roderick (2019) comes from the fitness of global ocean surface data. These equations are
 361 primarily calibrated to match observed evaporation rates, while the underlying process is
 362 generally overlooked.

363 In Section 2.1, it was suggested that $\Delta_D = 0$ for the saturated air while $\Delta_D \approx Q$ for the
 364 non-saturated air. In theory, it is expected that the transition track between saturated and
 365 non-saturated states should be continuous and smooth. That is, the changes in the value
 366 of Δ_D between the saturated (0) and non-saturated (Q) states should follow the variations
 367 in air energy and moisture (Figure 7). Since the relative humidity (RH) includes both
 368 information on air temperature and humidity, here we introduce a possible track of Δ_D
 369 depending on RH as: $\Delta_D = \psi(\text{RH}) \cdot Q$. As we expect, the value of Δ_D approaches 0 when
 370 the air is very moist (i.e., very close to the saturated state and RH close to 1), so ψ should
 371 be a nonlinear and monotone convex function of RH. We give a possible expression of
 372 $\psi(\text{RH})$ as:

$$373 \quad \psi(\text{RH}) = 1 - \frac{1}{1 + m \times \left(\frac{\text{RH}_{\max} - \text{RH}}{\text{RH} - \text{RH}_{\min}} \right)^n} \quad (28)$$

374 where RH_{\max} is 1, and RH_{\min} is 0.6 (Mccoll and Tang, 2023) over the water surfaces. m
 375 and n are shape parameters. To make $\psi(\text{RH})$ simple, we fixed n at 1, and let m be 100.
 376 The relationship between $\psi(\text{RH})$ and RH can be viewed in Figure 7 (b). For a specific
 377 case that T at 18 °C, we show the changes in Bo and α with RH in Figure 7 (c)-(d).
 378 Although there is a dramatic shift in Bo or α , it appears when RH is at 0.95-1, which is

379 outside the vast majority of actual cases (RH is generally smaller than 0.9 on a monthly
 380 or longer scale). After the shift point, with RH decreases, $\psi(\text{RH})$, B_0 , and α remain
 381 roughly stable. It is worth noting that Equation (28) (with specific parameters) is one
 382 possible case that connects the transition between saturated and non-saturated air states,
 383 a fine determination may be affected by local conditions, but Δ_D value around Q is
 384 expected for most of the cases.



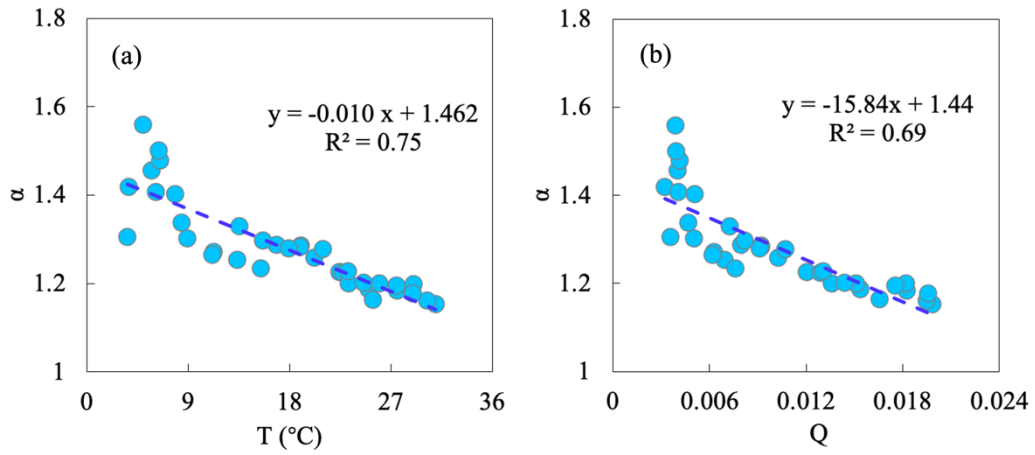
385
 386 Figure 7. (a) Transition between saturated and non-saturated air states. The filled circle
 387 represents one case in which the air is saturated (saturated state) and the open circle
 388 represents one case in which air is not saturated (non-saturated state). (b) Relationship
 389 between $\psi(\text{RH})$ and RH with Equation (28). (c)-(d) Changes in B_0 and α as the
 390 function of RH when air temperature is fixed at 18 $^{\circ}\text{C}$.

391 We recommend utilizing the derived model under warm conditions, for example, when
 392 the air temperature exceeds zero, to account for the prerequisite of a well-mixed boundary
 393 layer. In extremely cold regions or seasons, the water surface temperature can be lower
 394 than the air temperature, resulting in a downward sensible heat flux (De Bruin, 1982).
 395 Under such circumstances, the boundary layers exhibit relative stability and may not
 396 reach a well-mixed state. Additionally, we advise adopting a temporal scale ranging from
 397 weekly to monthly when applying the derived model. This is because the potential VPD
 398 budget (the governing equation) may not be rapidly achieved, such as on a diurnal or daily
 399 basis. Furthermore, over a longer term, the sensible heat flux typically manifests as
 400 upward in the majority of scenarios than on a fine temporal scale.

401 The derived formula for α has important practical meanings. For example, it would be
402 useful for estimating water surface evaporation and actual evapotranspiration based on
403 the PT model (Miralles et al., 2011; Maes et al., 2019). It can also help to constrain the
404 relationships among α , T, and Q in the complementary relationship, whose performance
405 previously depended on the inversed α (Liu et al., 2016). Besides, considering the impacts
406 of changing climate on α can significantly improve the performance of the hydrologic
407 model in runoff simulations and predictions (Pimentel et al., 2023).

408

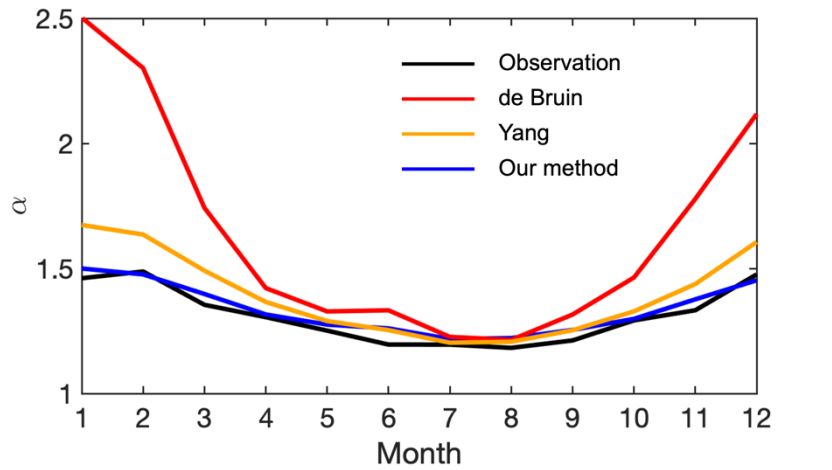
409 **Appendix A.**



410

411 Figure A1. Relationships of α with (a) temperature (T) and with (b) specific humidity (Q)
 412 on the ten-day scale using water surface observations collected over Lake Taihu.

413



414

415 Figure A2. Observed (black) and estimated α over lake Taihu. The blue line is α
 416 estimated with our method, and the red and orange lines are with two revised PT
 417 equations. The red line represents $\alpha = 1 + \frac{20}{\frac{\Delta}{\Delta + \gamma} (R_n - G)}$ (De Bruin and Holtslag, 1982), and

418

the orange line represents $\alpha = \frac{\Delta + \gamma}{\Delta + 0.24\gamma}$ (Yang and Roderick, 2019).

419

420 Table A1. Sensitivity of α to temperature (T) and specific humidity (Q) on the ten-day
 421 scale.

$d\alpha/dT$ ($^{\circ}\text{C}$)		$d\alpha/dQ$	
regression	derivation	regression	derivation
-0.010	-0.011	-15.84	-18.12

422

423 **Author Contributions**

424 Conceptualization: Ziwei Liu, Hanbo Yang. Data curation: Ziwei Liu. Formal analysis:
425 Ziwei Li. Funding acquisition: Hanbo Yang. Methodology: Ziwei Liu, Hanbo Yang.
426 Software: Ziwei Liu. Supervision: Hanbo Yang. Writing – original draft: Ziwei Liu.
427 Writing – review & editing: Changming Li, Taihua Wang, Hanbo Yang.

428 **Data availability**

429 Data of Lake Taihu can be obtained from Harvard Dataverse,
430 <https://doi.org/10.7910/DVN/HEWCWM>. The data of Poyang Lake can be obtained
431 from Zhao and Liu (2018) and Gan and Liu (2020). The data of Erhai can be obtained
432 from Du et al. (2018). The data of Guandu can be obtained from Zhao et al. (2019). The
433 data of Suwa lake can be obtained from the AsiaFlux
434 (http://asiaflux.net/index.php?page_id=1355). FluxNet 2015 data are available at
435 <https://fluxnet.fluxdata.org/data/download-data/>. CMIP6 data can be obtained from
436 Earth System Grid Federation (<https://esgf-node.llnl.gov>).

437 **Acknowledgments**

438 This study is financially supported by the National Natural Science Foundation of China
439 (grant nos. 51979140, 42041004).

440 **Competing interests**

441 There are no competing interests.

442 **References:**

- 443 Andreas, E. L. and Cash, B. A.: A new formulation for the Bowen ratio over saturated surfaces, *Journal of*
444 *Applied Meteorology*, 35, 1279-1289, 10.1175/1520-0450(1996)035<1279:anfftb>2.0.co;2, 1996.
- 445 Assouline, S., Li, D., Tyler, S., Tanny, J., Cohen, S., Bou-Zeid, E., Parlange, M., and Katul, G. G.: On the
446 variability of the Priestley-Taylor coefficient over water bodies, *Water Resources Research*, 52, 150-163,
447 10.1002/2015wr017504, 2016.
- 448 Bowen, I. S.: The ratio of heat losses by conduction and by evaporation from any water surface, *Physical*
449 *Review*, 27, 779-787, 10.1103/PhysRev.27.779, 1926.
- 450 Brutsaert, W. and Stricker, H. J. W. r. r.: An advection-aridity approach to estimate actual regional
451 evapotranspiration, 15, 443-450, 1979.
- 452 Crago, R. D., Szilagyi, J., and Qualls, R. J.: What is the Priestley–Taylor wet-surface evaporation parameter?
453 Testing four hypotheses, *Hydrol. Earth Syst. Sci.*, 27, 3205-3220, 10.5194/hess-27-3205-2023, 2023.
- 454 De Bruin, H. and Holtslag, A.: A simple parameterization of the surface fluxes of sensible and latent heat
455 during daytime compared with the Penman-Monteith concept, *Journal of Applied Meteorology and*
456 *Climatology*, 21, 1610-1621, 1982.
- 457 de Bruin, H. A. R.: Temperature and energy balance of a water reservoir determined from standard weather
458 data of a land station, *Journal of Hydrology*, 59, 261-274, [https://doi.org/10.1016/0022-1694\(82\)90091-9](https://doi.org/10.1016/0022-1694(82)90091-9),
459 1982.
- 460 Debruin, H. A. R. and Keijman, J. Q.: Priestley-taylor evaporation model applied to a large, shallow lake
461 in the netherlands, *Journal of Applied Meteorology*, 18, 898-903, 10.1175/1520-
462 0450(1979)018<0898:tptema>2.0.co;2, 1979.
- 463 Du, Q., Liu, H. Z., Liu, Y., Wang, L., Xu, L. J., Sun, J. H., and Xu, A. L.: Factors controlling evaporation
464 and the CO₂ flux over an open water lake in southwest of China on multiple temporal scales, *International*
465 *Journal of Climatology*, 38, 4723-4739, 10.1002/joc.5692, 2018.
- 466 Eichinger, W. E., Parlange, M. B., and Stricker, H.: On the concept of equilibrium evaporation and the value
467 of the Priestley-Taylor coefficient, *Water Resources Research*, 32, 161-164, 1996.
- 468 Gan, G. and Liu, Y.: Heat Storage Effect on Evaporation Estimates of China's Largest Freshwater Lake,
469 125, e2019JD032334, <https://doi.org/10.1029/2019JD032334>, 2020.
- 470 Greve, P., Roderick, M. L., Ukkola, A. M., and Wada, Y.: The aridity Index under global warming,
471 *Environmental Research Letters*, 14, 10.1088/1748-9326/ab5046, 2019.
- 472 Guo, X., Liu, H., and Yang, K. J. B.-L. M.: On the application of the Priestley–Taylor relation on sub-daily
473 time scales, 156, 489-499, 2015.
- 474 Han, S. and Guo, F.: Evaporation From Six Water Bodies of Various Sizes in East Asia: An Analysis on
475 Size Dependency, *Water Resources Research*, 59, 10.1029/2022wr032650, 2023.
- 476 Hicks, B. B. and Hess, G. D.: On the Bowen Ratio and Surface Temperature at Sea, *Journal of Physical*
477 *Oceanography*, 7, 141-145, 10.1175/1520-0485(1977)007<0141:otbras>2.0.co;2, 1977.
- 478 Jury, W. and Tanner, C. J. A. J.: Advection Modification of the Priestley and Taylor Evapotranspiration
479 Formula 1, 67, 840-842, 1975.
- 480 Lee, X., Liu, S., Xiao, W., Wang, W., Gao, Z., Cao, C., Hu, C., Hu, Z., Shen, S., Wang, Y., Wen, X., Xiao,
481 Q., Xu, J., Yang, J., and Zhang, M.: THE TAIHU EDDY FLUX NETWORK An Observational Program on
482 Energy, Water, and Greenhouse Gas Fluxes of a Large Freshwater Lake, *Bulletin of the American*
483 *Meteorological Society*, 95, 1583-1594, 10.1175/bams-d-13-00136.1, 2014.

- 484 Lhomme, J. P.: An examination of the Priestley-Taylor equation using a convective boundary layer model,
485 *Water Resources Research*, 33, 2571-2578, 1997a.
- 486 Lhomme, J. P.: A theoretical basis for the Priestley-Taylor coefficient, *Boundary-Layer Meteorology*, 82,
487 179-191, 1997b.
- 488 Liu, X., Liu, C., and Brutsaert, W.: Regional evaporation estimates in the eastern monsoon region of China:
489 Assessment of a nonlinear formulation of the complementary principle, 52, 9511-9521,
490 <https://doi.org/10.1002/2016WR019340>, 2016.
- 491 Liu, Z. and Yang, H.: Estimation of Water Surface Energy Partitioning With a Conceptual Atmospheric
492 Boundary Layer Model, *Geophysical Research Letters*, 48, e2021GL092643,
493 <https://doi.org/10.1029/2021GL092643>, 2021.
- 494 Liu, Z., Han, J., and Yang, H.: Assessing the ability of potential evaporation models to capture the sensitivity
495 to temperature, *Agricultural and Forest Meteorology*, 317, 108886, 2022.
- 496 Maes, W. H., Gentine, P., Verhoest, N. E. C., and Miralles, D. G.: Potential evaporation at eddy-covariance
497 sites across the globe, *Hydrology and Earth System Sciences*, 23, 925-948, 10.5194/hess-23-925-2019,
498 2019.
- 499 McColl, K. A. and Tang, L. I.: An analytic theory of near-surface relative humidity over land, *Journal of*
500 *Climate*, <https://doi.org/10.1175/JCLI-D-23-0342.1>, 2023.
- 501 McNaughton, K. and Spriggs, T.: A MIXED-LAYER MODEL FOR REGIONAL EVAPORATION,
502 *Boundary-Layer Meteorology*, 34, 243-262, 10.1007/bf00122381, 1986.
- 503 Miralles, D. G., Holmes, T., De Jeu, R., Gash, J., Meesters, A., Dolman, A. J. H., and Sciences, E. S.: Global
504 land-surface evaporation estimated from satellite-based observations, 15, 453-469, 2011.
- 505 Penman, H. L.: Natural evaporation from open water, bare soil and grass, *Proceedings of the Royal Society*
506 *of London Series a-Mathematical and Physical Sciences*, 193, 120-145, 10.1098/rspa.1948.0037, 1948.
- 507 Pimentel, R., Arheimer, B., Crochemore, L., Andersson, J. C. M., Pechlivanidis, I. G., and Gustafsson, D.:
508 Which Potential Evapotranspiration Formula to Use in Hydrological Modeling World-Wide?, 59,
509 e2022WR033447, <https://doi.org/10.1029/2022WR033447>, 2023.
- 510 Priestley, C. H. B. and Taylor, R. J.: Assessment of surface heat-flux and evaporation using large-scale
511 parameters, *Monthly Weather Review*, 100, 81-92, 10.1175/1520-0493(1972)100<0081:otaosh>2.3.co;2,
512 1972.
- 513 Raupach, M. R.: Equilibrium evaporation and the convective boundary layer, *Boundary-Layer Meteorology*,
514 96, 107-141, 10.1023/a:1002675729075, 2000.
- 515 Raupach, M. R.: Combination theory and equilibrium evaporation, *Quarterly Journal of the Royal*
516 *Meteorological Society*, 127, 1149-1181, 10.1002/qj.49712757402, 2001.
- 517 Roderick, M. L., Sun, F., Lim, W. H., and Farquhar, G. D.: A general framework for understanding the
518 response of the water cycle to global warming over land and ocean, *Hydrology and Earth System Sciences*,
519 18, 1575-1589, 10.5194/hess-18-1575-2014, 2014.
- 520 Shuttleworth, W. J.: *Evaporation In: Maidment, DR Handbook of hydrology*, 1993.
- 521 Slatyer, R. O. and McIlroy, I. C.: *Practical microclimatology: with special reference to the water factor in*
522 *soil-plant-atmosphere relationships*, Melbourne: Commonwealth Scientific and Industrial Research
523 Organisation.1961.
- 524 Su, Q. and Singh, V. P.: Calibration-Free Priestley-Taylor Method for Reference Evapotranspiration
525 Estimation, 59, e2022WR033198, <https://doi.org/10.1029/2022WR033198>, 2023.
- 526 Taoka, T., Iwata, H., Hirata, R., Takahashi, Y., Miyabara, Y., and Itoh, M.: Environmental Controls of
527 Diffusive and Ebullitive Methane Emissions at a Subdaily Time Scale in the Littoral Zone of a Midlatitude
528 Shallow Lake, *Journal of Geophysical Research-Biogeosciences*, 125, 10.1029/2020jg005753, 2020.

529 Thornthwaite, C. W. and Holzman, B.: Evaporation from land and water surfaces, *Monthly Weather Review*,
530 67, 4-11, 10.1175/1520-0493(1939)67<4:doefl>2.0.co;2, 1939.

531 van Heerwaarden, C. C., de Arellano, J. V. G., Moene, A. F., and Holtslag, A. A. M.: Interactions between
532 dry-air entrainment, surface evaporation and convective boundary-layer development, *Quarterly Journal of*
533 *the Royal Meteorological Society*, 135, 1277-1291, 10.1002/qj.431, 2009.

534 Xiao, W., Zhang, Z., Wang, W., Zhang, M., Liu, Q., Hu, Y., Huang, W., Liu, S., and Lee, X.: Radiation
535 Controls the Interannual Variability of Evaporation of a Subtropical Lake, *Journal of Geophysical Research-*
536 *Atmospheres*, 125, 10.1029/2019jd031264, 2020.

537 Yang, Y. and Roderick, M. L.: Radiation, surface temperature and evaporation over wet surfaces, *Quarterly*
538 *Journal of the Royal Meteorological Society*, 145, 1118-1129, 10.1002/qj.3481, 2019.

539 Zhao, J., Zhang, M., Xiao, W., Wang, W., Zhang, Z., Yu, Z., Xiao, Q., Cao, Z., Xu, J., Zhang, X., Liu, S.,
540 and Lee, X.: An evaluation of the flux-gradient and the eddy covariance method to measure CH₄, CO₂, and
541 H₂O fluxes from small ponds, *Agricultural and Forest Meteorology*, 275, 255-264,
542 10.1016/j.agrformet.2019.05.032, 2019.

543 Zhao, X. and Liu, Y.: Variability of Surface Heat Fluxes and Its Driving Forces at Different Time Scales
544 Over a Large Ephemeral Lake in China, *Journal of Geophysical Research-Atmospheres*, 123, 4939-4957,
545 10.1029/2017jd027437, 2018.

546